



HAL
open science

Space Weathering Affects the Remote Near-IR Identification of Phyllosilicates

Stefano Rubino, Cateline Lantz, Donia Baklouti, Hugues Leroux, Ferenc Borondics, Rosario Brunetto

► **To cite this version:**

Stefano Rubino, Cateline Lantz, Donia Baklouti, Hugues Leroux, Ferenc Borondics, et al.. Space Weathering Affects the Remote Near-IR Identification of Phyllosilicates. *The Planetary Science Journal*, 2020, 1 (3), pp.61. 10.3847/psj/abb94c . hal-03134243

HAL Id: hal-03134243

<https://hal.univ-lille.fr/hal-03134243v1>

Submitted on 8 Feb 2021

HAL is a multi-disciplinary open access archive for the deposit and dissemination of scientific research documents, whether they are published or not. The documents may come from teaching and research institutions in France or abroad, or from public or private research centers.






L'archive ouverte pluridisciplinaire **HAL**, est destinée au dépôt et à la diffusion de documents scientifiques de niveau recherche, publiés ou non, émanant des établissements d'enseignement et de recherche français ou étrangers, des laboratoires publics ou privés.



Distributed under a Creative Commons Attribution 4.0 International License



Space Weathering Affects the Remote Near-IR Identification of Phyllosilicates

Stefano Rubino¹ , Cateline Lantz¹ , Donia Baklouti¹ , Hugues Leroux² , Ferenc Borondics³, and Rosario Brunetto¹ 

¹Institut d'Astrophysique Spatiale, Université Paris-Saclay, CNRS, F-91405, Orsay, France; stefano.rubino@ias.u-psud.fr

²Univ. Lille, CNRS, INRAE, ENSCL, Centrale Lille, UMR 8207—Unité Matériaux et Transformations, F-59000 Lille, France

³SMIS Beamline, SOLEIL Synchrotron, BP48, L'Orme des Merisiers, F-91192 Gif sur Yvette Cedex, France

Received 2020 June 1; revised 2020 September 2; accepted 2020 September 15; published 2020 November 6

Abstract

Near-infrared (NIR) spectrometers on board current sample return missions Hayabusa2 and the Origins-Spectral Interpretation-Resource Identification-Security-Regolith Explorer (OSIRIS-REx) from primitive bodies detected the presence of hydrated silicates on the surface of asteroids Ryugu and Bennu, respectively. These detections relied upon the study of the 2.7 μm OH-stretching spectral feature, whose peak position is related to the composition and structure of minerals. However, space weathering might alter the band profile, depth and position, thus complicating the interpretation of remote sensing data. In order to better understand these processes and provide support to space missions, we performed ion bombardment experiments on serpentine and saponite analogs. These two phyllosilicates are among the dominant mineral phases found in hydrated carbonaceous chondrites, which are possible analogs to surface materials observed on these primitive asteroids. We studied the behavior of the 2.7 μm band as a function of ion fluence and found that the evolution of the phyllosilicate depends on its nature. For the saponite sample, the band is only slightly affected by ion bombardment, while for both serpentine samples it shifts toward longer wavelengths. For both samples, peak intensity and width is not strongly affected. The band shift for serpentine indicates that space weathering introduces a bias in the interpretation of NIR remote sensing observations of phyllosilicates. The shift observed in our experiments can be detected by instruments on board Hayabusa2 and OSIRIS-REx, depending on the geometry of observation. Our findings provide support to the interpretation of such data.

Unified Astronomy Thesaurus concepts: [Space weather \(2037\)](#); [Spectroscopy \(1558\)](#); [Near infrared astronomy \(1093\)](#); [Infrared astronomy \(786\)](#); [Laboratory astrophysics \(2004\)](#); [Small solar system bodies \(1469\)](#); [Surface composition \(2115\)](#); [Surface processes \(2116\)](#)

1. Introduction

The study of hydrated silicates in small bodies, as tracers of aqueous alteration, is of utmost importance for understanding the evolution of primitive materials in the early solar system. Two sample return missions have been launched to study asteroids expected to have undergone aqueous alteration: the Hayabusa2 mission Japan Aerospace Exploration Agency (JAXA) targeting C-type asteroid 162173 Ryugu (Watanabe et al. 2017) and the Origins-Spectral Interpretation-Resource Identification-Security-Regolith Explorer (OSIRIS-REx) mission (NASA) targeting B-type asteroid 101955 Bennu (Lauretta et al. 2017). The detection of hydration on the asteroids' surfaces can be achieved by remote sensing in the near-infrared (NIR) spectral range, using the 2.7 μm band of phyllosilicates. This feature is attributed to the stretching vibration of hydroxyl groups (O-H) covalently bonded to metallic atoms (M) of octahedral MO₆ sites. Its position and shape are sensitive to the mineral's composition and structure (Madejová et al. 2017). In particular, the peak position has been well studied in terrestrial phyllosilicates as a function of the Mg/Fe ratio, with wavelengths shorter for Mg-rich than for Fe-rich compositions (Farmer 1974; Besson & Drits 1997; Bishop et al. 2008). The 2.7 μm band has been measured in aqueously altered carbonaceous chondrites (Zolensky & McSween 1988; Miyamoto & Zolensky 1994), and also detected on asteroids despite telluric

absorption (Lebofsky 1978; Rivkin et al. 2002). More recently, this feature has been observed by the Dawn mission on the dwarf planet Ceres (de Sanctis et al. 2015) and by Hayabusa2 and OSIRIS-REx on Ryugu and Bennu (Hamilton et al. 2019; Kitazato et al. 2019).

Atmosphere-less bodies in our solar system are known to be affected by space weathering (SpWe). This phenomenon includes multiple processes, such as micrometeorite bombardment, high-energy cosmic and solar ion bombardment, and low-energy solar wind bombardment (Beth Ellen Clark et al. 2002; Brunetto et al. 2015). Understanding the relative rates of all SpWe processes and their optical effects has been challenging for quite awhile (Clark et al. 2002). The spectroscopic and microscopic studies of the Hayabusa mission (JAXA) showed that solar wind should be the main source of surface weathering in the inner solar system (Noguchi et al. 2014). At this short distance from the Sun, solar wind is the main source of rapid (10^4 – 10^6 yr) weathering, while the effects caused by micrometeorite bombardment act on a longer timescale (10^8 yr; Brunetto et al. 2015). Heating processes are also known to affect the surface properties of asteroids. Marchi et al. (2009) discussed how episodes of strong solar heating could have partly removed volatiles components from near-Earth orbits (NEOs) asteroids surfaces. Regarding primitive NEOs in particular, like C-type asteroids, the effects on the hydration features are expected to be more severe. However, Marchi et al. also point out that data collected until now is not unambiguous enough to explain the difference of the NEOs hydration features solely on solar heating. Thermal fatigue caused by solar heating can also affect the surface properties of



Original content from this work may be used under the terms of the [Creative Commons Attribution 4.0 licence](#). Any further distribution of this work must maintain attribution to the author(s) and the title of the work, journal citation and DOI.

Table 1
Composition of the Samples Used in This Study

	Serpentine UB-N SARM ^a	Serpentine UB-N	Serpentine Rawhide	Saponite
SiO ₂	45.25 ± 0.18	45.46 ± 0.33	45.81 ± 0.32	48.98 ± 0.31
Al ₂ O ₃	3.33 ± 0.09	3.32 ± 0.17	0.89 ± 0.10	14.77 ± 0.17
MgO	40.41 ± 0.22	40.59 ± 0.40	45.78 ± 0.19	9.90 ± 0.15
FeO–Fe ₂ O ₃	9.22 ± 0.35	9.26 ± 0.25	6.66 ± 0.25	13.84 ± 0.24
CaO	1.37 ± 0.04	1.36 ± 0.10	nd	7.08 ± 0.13
TiO ₂	0.13 ± 0.01	nd	nd	0.84 ± 0.09
Cr ₂ O ₃	nd	nd	0.86 ± 0.15	nd
MnO	0.12 ± 0.01	nd	nd	0.37 ± 0.12
Na ₂ O	0.11 ± 0.04	nd	nd	3.95 ± 0.10
K ₂ O	0.02 ± 0.01	nd	nd	0.25 ± 0.04

Note. Compositions were obtained by the Scanning Electron Microscope–Energy-Dispersive X-ray Spectroscopy (SEM–EDX) measurements performed at the UMET lab, University of Lille.

^a The first column is the composition of the serpentine UB-N provided by the SARM. Uncertainties are given at 1σ. nd = not detected.

asteroids, governing regolith generation on small asteroids, thus contributing to the surface rejuvenation processes (Delbo et al. 2014). Overall, SpWe induces variations of the spectral properties of surface materials, including spectral reddening/blueing in the visible (Vis)–NIR range (Clark et al. 2001; Binzel et al. 2001; Hiroi et al. 2006; Lantz et al. 2013).

SpWe can be replicated on Earth through the use of ion irradiation and/or laser pulse experiments. Previous studies on carbonaceous chondrites (CCs) reported variations of IR bands upon ion bombardment, in both the NIR and MIR ranges (Vernazza et al. 2013; Lantz et al. 2015). In particular, in the experiment carried out by Lantz et al. (2017), the 2.7 μm band of CCs had been observed to change in shape as well as shift in position toward longer wavelengths after ion bombardment. However, Lantz et al. (2017) used spectral measurements acquired at atmospheric pressure. Thus, the presence of atmospheric water adsorbed on the surface of the studied samples might have affected the band shape above 2.8 μm, and its potential contribution to the reported global change cannot be excluded. In this paper we report new experimental results of ion bombardment on terrestrial phyllosilicates as a simulation of SpWe of atmosphere-less bodies rich in hydrated silicates. These experiments were performed in a vacuum chamber to simulate space conditions. We monitored the 2.7 μm feature before and after ion bombardment.

2. Samples and Methods

2.1. Sample Description and Preparation

The irradiation experiments were performed on serpentines and saponite. These minerals correspond to the major hydrated silicate phases found in CI- and CM-type chondrites (Brearley 2006; King et al. 2015) and may probably dominate at the surface of Ryugu and Bennu (Hamilton et al. 2019; Kitazato et al. 2019). The saponite sample is a griffithite (Fe-rich saponite), coming from Griffith Park in California. Two serpentine samples were used, labeled serpentine Rawhide and serpentine UB-N. Serpentine Rawhide is mostly antigorite with chrysotile veins and comes from the Rawhide mines in California. Serpentine UB-N comes from the Col des Bagenelles in France, structurally dominated by lizardite (Gayk & Kleinschrodt 2000). Chemical compositions of the samples were measured by energy dispersive X-ray spectroscopy (EDX; at 15 keV) on a scanning electron microscopy (SEM). The structural formulae were found as

following: Na_{0.5}Ca_{0.5}Mg_{1.0}Fe_{0.7}Al_{1.1}Si_{3.3}O₁₀(OH)₂ for saponite, Mg_{2.8}Fe_{0.2}Al_{0.04}Si_{1.9}O₅(OH)₄ for serpentine Rawhide, and Ca_{0.05}Mg_{2.6}Fe_{0.4}Al_{0.1}Si_{1.8}O₅(OH)₄ for serpentine UB-N. We summarize elemental composition information of our samples in Table 1. The two serpentine samples differ in their atomic ratio Fe/(Fe+Mg) content. The ratio is equal to 0.07 for serpentine Rawhide and to 0.13 for serpentine UB-N.

The sample preparation method and the experimental protocol were similar to previous ion bombardment studies, which were focused on carbonaceous chondrites (Brunetto et al. 2014; Lantz et al. 2015, 2017). The samples were crushed using an agate mortar. Since terrestrial rocks were used, the resulting powders cannot be considered perfectly pure. A low fraction of terrestrial organics together with some minor mineral phases are expected to be present (such as clinocllore in the saponite/griffithite and calcite in the serpentine UB-N). However, these impurities should not interfere with the 2.7 μm phyllosilicate feature. Although grain size was not constrained during the crushing process, the size range of each powdered sample was estimated using an SEM (at Unité Matériaux et Transformation, Université de Lille (UMET), France). The grain size of the powders is found in the range 1–100 μm for all samples. For each mineral sample, two pellets of 20 mm in diameter were prepared by pressing ~240 mg of powdered sample onto a PEG substrate (powdered polyethylene glycol with an average molecular mass of 8000 g/mol, from Fisher Scientific) for a duration of 5 minutes, under a weight of 7 tons. The phyllosilicate layer is thick enough (>500 μm) to avoid any ion (see the Stopping and Range of Ions in Matter (SRIM) results in Section 2.2) or photon (typically probing a layer of 2 μm in the 2–3 μm wavelength region for serpentines; see Brunetto et al. 2020) from interacting with the PEG substrate. Out of the six pellets, three underwent ion bombardment, while the remaining pellets were preserved as control samples, in case we needed more data regarding the “non-bombarded” state of our samples and to check for potential contamination/evolution over time.

2.2. Experimental Setup

We performed ion bombardment at room temperature in the Irradiation de Glaces et Météorites Analysées par Réflectance (IMGMAR, Vis–Institut d’Astrophysique Spatiale (IAS)–Centre de Sciences Nucléaires et de Sciences de la Matière (CSNSM), Orsay) vacuum chamber ($P \sim 10^{-7}$ mBar) interfaced to the SIDONIE implanter (CSNSM, Orsay) using He⁺ at

40 keV and ion fluences of 1×10^{16} , 3×10^{16} , and 6×10^{16} ions cm^{-2} . The ion flux was of $\sim 10^{13}$ ions/(s cm^2). The ion fluence was derived by a direct measurement of the ion current, thanks to a brass ring placed before the entrance of the vacuum chamber (Urso et al. 2020). The implantation depth in our samples was estimated by the SRIM code (Ziegler et al. 2010; see Brunetto et al. 2014 for details) to be of 360 ± 110 nm for the saponite and 310 ± 90 nm for the two serpentine samples. SRIM simulation results were obtained using composition results from our SEM–EDX measurements and densities from Skinner (1963) and Roberts et al. (1990).

The applicability of He^+ irradiation at 40 keV as a simulation of solar ion irradiation and its limitations are discussed by Brunetto et al. (2014) and Lantz et al. (2017). We summarize here the main points for the sake of clarity. Due to obvious limitations in time and resources, it is almost impossible to reproduce in the laboratory all the range of ion mass and energies affecting asteroid surfaces, so each study typically focuses on one particular component. Following previous studies (Brunetto et al. 2014; Lantz et al. 2015), we chose He^+ in order to simulate an important fraction of the ions in the solar wind. The particles emitted with the slow solar wind have energies ~ 1 keV/u and their flux decreases with the square of distance from the Sun. Hydrogen is the main component ($\sim 95\%$, average energy ~ 1 keV), and helium is the second most abundant species ($\sim 4.6\%$) with an average energy of ~ 4 keV. While the energy of 40 keV is close to the average energy for heavier ions present in the slow solar wind (such as Ar^+), it is also about 10 times higher than the average energy for He. However, higher-energy helium ions are also emitted from the Sun through active regions and solar flares. Their contribution to SpWe effects on airless bodies should not be neglected. For instance, Matsumoto et al. (2015) proposed that high-energy He^+ ions might have played a role in the formation of a thick space-weathered layer detected on an Itokawa particle. Using the energy spectra of ions from active regions and solar flares (e.g., Johnson 1990), Brunetto et al. (2014) estimated that the weathering timescales of asteroids by 40 keV He^+ are about 10 times longer than 4 keV He^+ . Of course, many more ion species and energies are involved in the weathering processes, so the 40 keV He^+ irradiations studied here are certainly not an exhaustive reproduction of asteroid SpWe.

The whole surface of each pellet was subjected to ion bombardment, with the exception of a small external corona ($\sim 500 \mu\text{m}$ in width), which is an area masked by the sample holder used to mount the samples vertically in the vacuum chamber. We acquired reflectance spectroscopy measurements in the NIR (0.96–4 μm) before and after each bombardment step, directly in the vacuum chamber. We used a Fourier Transform InfraRed spectrometer (Tensor37, Bruker) and a Vis–NIR optic fiber to collect light from the sample with an angle $e = 15^\circ$, while the illumination angle was $i = 20^\circ$ and the phase angle was 15° (because the incident and emission angles and the surface normal are not in the same plane; see Lantz et al. 2017). The illumination spot was about 12 mm in diameter while the collection spot size is ~ 4 mm.

To calibrate the absolute reflectance of our measurements, we acquired reference spectra in the vacuum chamber using a Spectralon standard (99% Lambertian reflectance, Labsphere). An additional reference measurement was performed on InfraGold (Labsphere), which allowed the correction of minor NIR features present in the Spectralon spectrum. The spectral resolution was 16 cm^{-1} , the spectral sampling was 8 cm^{-1} , and we accumulated 4096 scans per spectrum.

In addition to the vacuum spectra (referred to as *in situ*), we performed measurements under ambient conditions (*ex situ*) using two different setups. We acquired spectra on virgin pellets (the control samples) and on the ion bombarded ones with the highest fluence. They are reported in the Appendix. The Fourier transform infrared spectroscopy (FTIR) measurements reported in Figure A1 (right) were acquired with an Agilent Cary 670/620 microspectrometer installed at the SMIS beamline of the SOLEIL synchrotron (France). IR spectra were measured using the internal Global source, with respect to gold references. More details can be found in Brunetto et al. (2018). The FTIR spectra shown in Figure A1 (left) were acquired with a PerkinElmer point spectrometer, installed at the Institut d’Astrophysique Spatiale (France). An internal Global source was used, with respect to both the Spectralon and the InfraGold standard cited above. It is relevant to point out that the *ex situ* setups described above have different optical geometries: the Agilent microspectrometer uses an IR microscope (15x objective, N.A. = 0.62), while the PerkinElmer measures biconical reflectance.

3. Results

All spectra acquired before ion bombardment showed the 2.7 μm feature. We were able to distinguish certain differences in band shape and peak position among our samples due to their different composition and crystal structure (Figure 1).

The peak position of the 2.7 μm feature was estimated by applying different instances of a Savitzky–Golay filter to our spectra, then by determining the region of interest centered on our feature, computing the barycenter associated to this region of interest (ROI) (to account for the asymmetry of the spectral feature), and averaging the peak position of each Savitzky–Golay instance. The position of the feature computed on raw data (without denoising) was also included for the computation of the average position. The wavelength obtained by this algorithm was assimilated to the feature’s position. This method allowed us to extract the following band positions: 2746 ± 3 nm for the saponite, 2719 ± 5 nm for the serpentine UB-N, and 2711 ± 3 nm for the serpentine Rawhide. The peak position for the two serpentines is coherent with their composition: the feature of the serpentine Rawhide (slightly Mg-richer) is located at shorter wavelength compared to serpentine UB-N. All values are coherent with the peak position associated with the hydroxyl stretching of hydrated silicates in the reference spectra found in the literature for each sample (Rodriguez 1994 for the saponite; Bishop et al. 2008; Takir et al. 2013 for the serpentines).

It is important to address that the MO–H stretching band can incorporate multiple contributions depending on the complexity of the phyllosilicate sample. For instance, in saponite, interlayer H_2O molecules are expected to contribute to the general shape of the feature. This can be seen in our *in situ* spectra (Figure 1), where the general shape of the virgin saponite spectrum around 3–3.3 μm is deeper than for both virgin serpentines. Additionally, spectra acquired *ex situ* with the PerkinElmer point spectrometer and with the Agilent microscope (Figure A1) show the contribution of adsorbed atmospheric water at the surface of our samples; contribution that we were able to minimize in our *in situ* measurements on INGMAR since the samples were left in the vacuum chamber at $P \sim 10^{-7} \text{ mBar}$ for 8 hours before ion bombardment and remained there for the whole duration of the experiment.

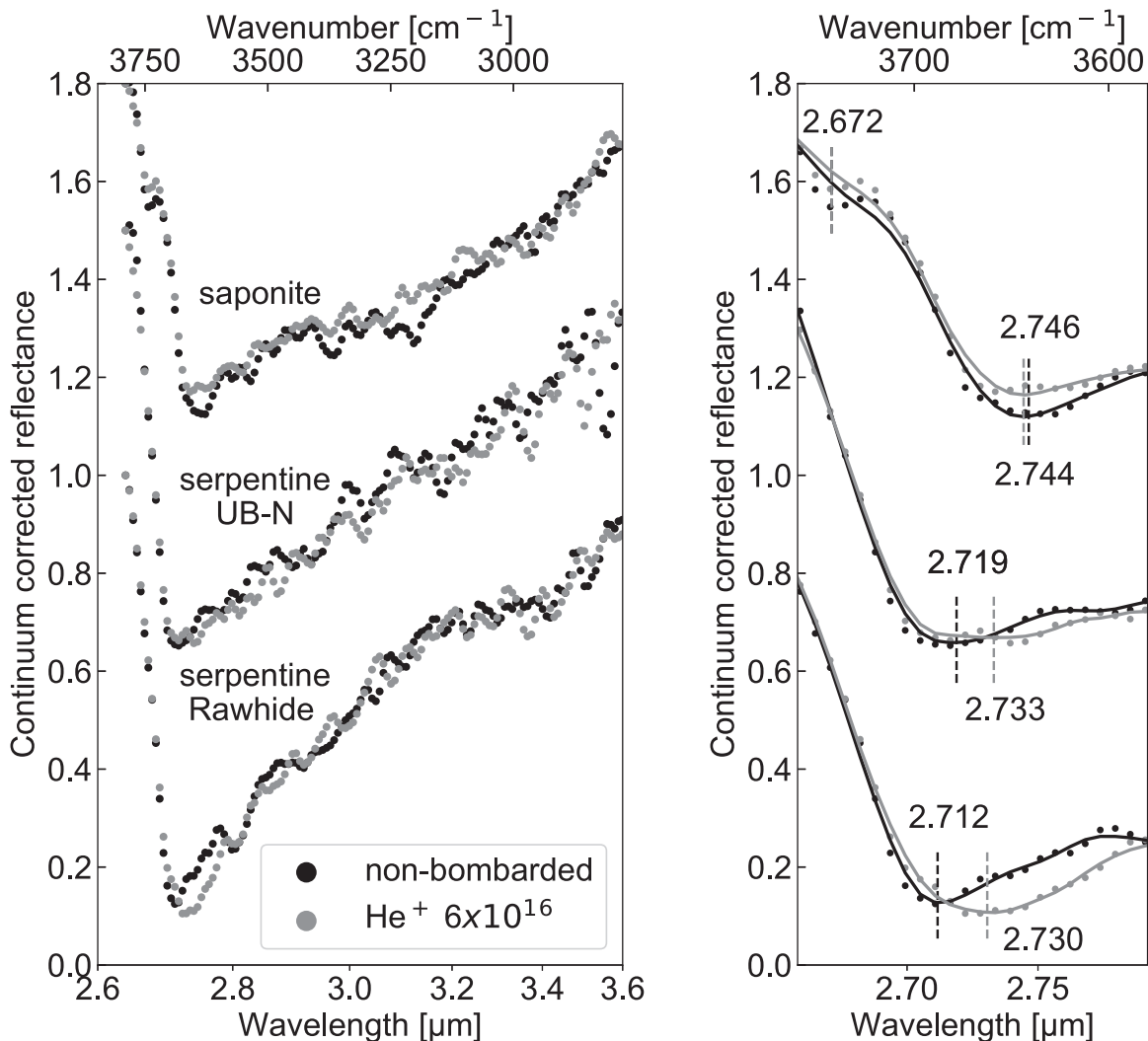


Figure 1. In situ evolution of the $2.7 \mu\text{m}$ feature before (non-bombarded; black dots) and after maximum ion fluence (6×10^{16} ions/cm 2 ; gray dots). Spectra were shifted for clarity. A linear continuum correction from $2.64 \mu\text{m}$ to $4 \mu\text{m}$ was applied. Solid lines represent the Savitzky–Golay filter used for denoising the spectra. For plotting, the linear scale is used with respect to wavenumbers. The right panel is a zoomed in on the region of the $2.7 \mu\text{m}$ bands.

After exposure to the maximum fluence (6×10^{16} ions/cm 2), the feature’s position for the serpentines changes as follows: 2733 ± 4 nm for the serpentine UB-N and 2730 ± 4 nm for the serpentine Rawhide. The newly measured position for the saponite feature is 2744 ± 5 nm, which hints that the peak’s position for the saponite does not change after bombardment within our error bars. The saponite sample also displays a small peak around 2672 nm (best visible in the zoomed-in panel of Figure 1), which originated from the Si-OH vibration mode (Trombetta et al. 2000). Ion bombardment does not affect its position. Finally, we notice that the band depth for both serpentines does not change within our error bars, while the saponite feature’s depth decreases ($-7 \pm 2\%$) and broadens slightly. Overall, ion bombardment processes do not seem to significantly alter the intensity and shape of the $2.7 \mu\text{m}$ feature in phyllosilicates, and its effects can mostly be found in the evolution of the feature’s position.

The evolution of the phyllosilicate band position as a function of ion fluence is reported in Figure 2. Serpentine Rawhide shows clear evidence of a MO-H band position gradual shift toward longer wavelengths with increasing bombardment fluence (small error bars due to the narrow shape of the feature). At the end of the

experiment, the measured shift was 19 ± 3 nm for serpentine Rawhide and 14 ± 3 nm for serpentine UB-N. The evolution with increasing fluence amount for the serpentine UB-N and the saponite is more difficult to assert due to the broader shape of the feature for these samples, which affects the error associated with the computed position. Nonetheless, two different behaviors emerge clearly: the MO-H feature for both serpentines shifts toward longer wavelengths, while the peak position of the saponite does not change within our error bars, except for the measurement acquired in medium ion fluence (3×10^{16} ions/cm 2), which was a particularly noisy acquisition compared to all other experiments.

The effects upon ion bombardment have been also measured ex situ, for samples irradiated at 6×10^{16} ions/cm 2 with two other instruments (see Section 2). The spectral shifts, measured ex and in situ, are compared in Figure 3.

The ex situ spectral shifts are different from the ones measured in situ (INGMAR). We interpret these differences as an effect of the different optical geometries for the three measurements (see Section 4). Nonetheless, these ex situ results are coherent with the two tendencies identified in the in situ spectra, since in both serpentines, a spectral shift can be identified, contrary to the saponite sample.

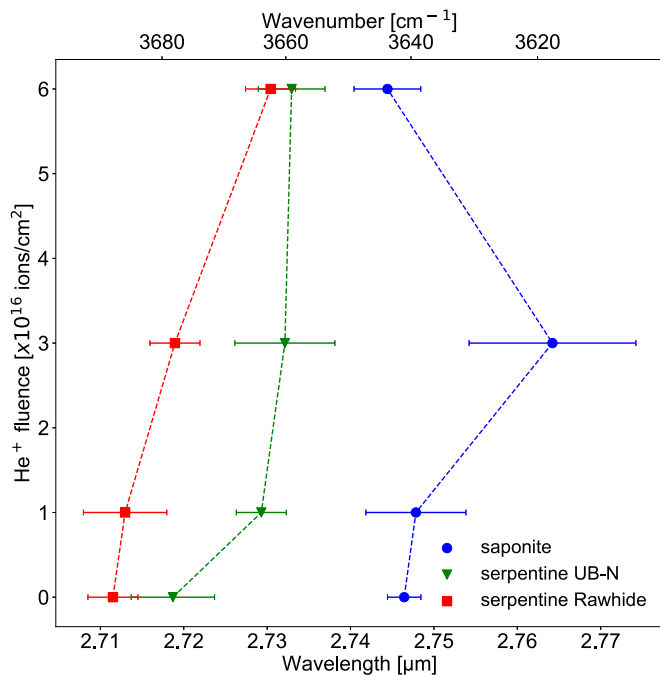


Figure 2. In situ evolution of the $2.7 \mu\text{m}$ feature peak position of the studied phyllosilicates upon irradiation. Saponite is in blue circles, serpentine UB-N is in green triangles, and serpentine Rawhide is in red squares. The irradiation fluence 0 refers to the samples before ion bombardment.

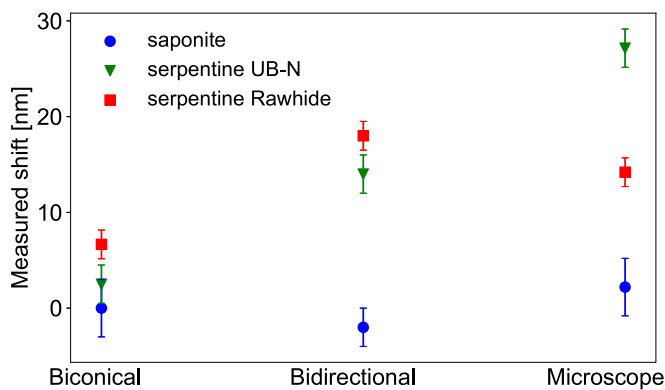


Figure 3. Comparing the bombardment-induced spectral shift of the MO-H feature measured with different optical geometries (associated to different instruments): biconical reflection (PerkinElmer point spectrometer), bidirectional reflection (INGMAR setup), and microscope reflection (Agilent IR microscope). Same color/symbol code as in Figure 2.

4. Discussion

Contrary to other IR bands of phyllosilicates that are coupled to other vibrations of the structure, the O-H stretching band is completely separated and is only affected by the immediate vicinity of the hydroxyl group (Farmer 1974). The samples we chose for this study belong to two different classes of phyllosilicates that correspond to two distinct types of crystal structure. In the saponite subgroup the octahedral layer containing metals bonded to hydroxyl groups (O-H) is covalently bonded to the oxygens of the tetrahedral Si-O layers that are both above and below it. The different layers are arranged to form a tetrahedral-octahedral-tetrahedral (TOT) unit separated from the following by an interlayer of water molecules (and possibly cations; Mitra et al. 2013). That way, each TOT unit almost behaves as a separate entity, the lattice stress induced by He^+

bombardment is relaxed at the scale of the TOT unit, and the immediate environment of each hydroxyl group cannot be disturbed easily. In serpentines, the octahedral layer containing metals bonded to O-H is covalently bonded to a single Si-O layer, creating an TO structure, while hydrogen bindings provide cohesion with the Si-O layer of the adjacent TO layer (Auzende 2003). No water interlayer separates each TO layer. Any stress on the TO layer or the adjacent one will affect the hydrogen bindings and will disturb the crystal lattice of the serpentine (similarly to what observed by Leroux et al. 2019 in olivines), affecting the immediate environment of the MO-H groups, which in turn, will impact the position of the $2.7 \mu\text{m}$ band. This crystal structure difference may explain why the $2.7 \mu\text{m}$ band position of the serpentine samples is more affected than the saponite sample in our experiments. Compositional-related processes, such as local variations of the $\text{Fe}/(\text{Mg}+\text{Fe})$ ratio, preferential amorphization of Mg-rich phyllosilicates, or preferential sputtering of Mg (Hapke et al. 1975), could also affect the position of the feature upon bombardment. Scanning electron microscopy (SEM) and transmission electron microscopy (TEM) measurements will be performed in a forthcoming study on all our samples to investigate the effects of ion bombardment at a nanometric scale.

Ion bombardment does not seem to greatly affect the shape or intensity of the $2.7 \mu\text{m}$ feature. In our case, both serpentines' hydration peaks retained the same shape and intensity, despite the spectral shift. For the saponite sample, a slight decrease in intensity ($-7 \pm 2\%$) as well as a light broadening of the feature seems to occur. No particular tendency regarding the intensity or shape emerges in the in situ measurements at intermediate fluences, but the in situ changes between non-bombarded samples and samples bombarded at maximum fluence are consistent with the changes observed in the ex situ spectra (Figure A1). In particular, the measurements acquired with biconical reflectance (PerkinElmer point spectrometer, as seen in left panel in Figure A1) clearly show the decrease in intensity for the saponite sample, while no changes can be observed for the serpentine samples.

We measured the shift after ion bombardment with three instruments, each with a different optical geometry (Figure 3). The PerkinElmer point spectrometer measures biconical reflectance, and an off-axis mount greatly decreases the contribution of specular reflectance in the associated measurements. The INGMAR setup measures bidirectional reflectance (with a phase angle of $\varphi = 15^\circ$), similarly to how the OVIRS (OSIRIS-REx Visible and InfraRed Spectrometer) and NIRS3 (Near Infrared Spectrometer) instruments operate on board OSIRIS-REx and Hayabusa2. Finally, the Agilent spectrometer is interfaced with an IR microscope. We notice that there is a sort of “inversion” between the two serpentines when comparing the measured shifts with the INGMAR setup and the Agilent microscope. Overall, the effect of spectral band shift is more easily detected at certain geometries probably because photons penetrate less and thus better probe the upper irradiated layers. Indeed, previous studies have shown that as the phase angle increases, the mean path of photons probing the sample surface also increases (Adams & Filice 1967), which hints that the contribution of volume scattering with respect to surface scattering gets more important. In the case of remote sensing of asteroid surfaces, this implies that the spectral shift would be more easily detected in observations performed at small phase angles. This scenario can be verified in data

collected by Hayabusa2 and OSIRIS-REx, when a given terrain is observed at different geometries during the mission.

In this new study, the in situ spectra were acquired in a vacuum chamber. This, and the fact that our detection relies on bidirectional reflection, allowed us to acquire measurements in conditions comparable to the remote sensing measurements acquired by Hayabusa2 and OSIRIS-REx orbiting Ryugu and Bennu respectively. Thus our spectra may provide support to the interpretation of remote sensing data of these two missions. Our results imply that SpWe may induce a bias in the interpretation of NIR remote sensing observations of phyllosilicates on planetary surfaces. The $2.7\ \mu\text{m}$ feature is generally used as a remote sensing proxy to determine the Mg-to-Fe ratio of phyllosilicates (Sabins 1999; Bishop et al. 2008). Since ion bombardment induces for certain minerals a shift of the $2.70\text{--}2.72\ \mu\text{m}$ feature toward longer wavelengths, the estimation of the composition of hydrated minerals will be biased on space-weathered surfaces.

The maximum spectral shift observed in our measurements in the vacuum chamber is $19 \pm 3\ \text{nm}$ for the serpentine Rawhide (Mg-rich serpentine), which is a value that can be detected in the data acquired by the NIRS3/Hayabusa2 (spectral sampling of $\sim 18\ \text{nm}$; Iwata et al. 2017) and the OVIRS/OSIRIS-REx (spectral sampling of $\sim 10\ \text{nm}$; Christensen et al. 2018) instruments. The phyllosilicate peak position observed on Ryugu and Bennu is about $2.72\ \mu\text{m}$ and $2.74\ \mu\text{m}$, respectively, and its position is quite homogeneous all across the asteroids' surface (Kitazato et al. 2019; Hamilton et al. 2020). The peak positions of the two asteroids are compatible both with irradiated or unirradiated phyllosilicates of different composition, and it is not possible to discriminate the two scenarios based on the average peak position only. However, our laboratory results definitely support the idea that, if solar wind is the dominant SpWe process for young ($<10^7$ years) surfaces in the inner solar system, as suggested by many authors (e.g., Vernazza et al. 2009; Noguchi et al. 2014; Bonal et al. 2015), the least altered terrains on Ryugu and Bennu may be characterized by positions of the $2.7\ \mu\text{m}$ feature peaking at shorter wavelengths than the oldest (more altered) terrains (Lantz et al. 2017). The Small Carry-on Impactor (SCI) crater experiment on board Hayabusa2 (Arakawa et al. 2020) has provided an excellent test of this hypothesis (Kitazato et al. 2020), as it has produced a fresh crater at the surface of Ryugu. In the case of older surfaces ($>10^8$ years), the effect of solar wind irradiation would tend to saturate, and spectral differences among different terrains would be limited, while other competitive processes such as micrometeorite bombardments or heating processes would contribute significantly.

5. Conclusions

The laboratory reproduction of solar wind irradiation provides the community with relevant data for the interpretation of SpWe effects on the surface of primitive asteroids. The irradiation-induced changes of the $2.7\text{--}2.8\ \mu\text{m}$ phyllosilicate feature depend on the phyllosilicate nature. Serpentine have their $2.7\ \mu\text{m}$ feature modified by ion irradiation, both in the profile and peak position, whereas saponite bands do not significantly change position after irradiation and only show a limited reduction of the band intensity. Our experiments suggest that SpWe may induce a bias in the spectral interpretation of NIR remote sensing observations of asteroids, which is an effect that is within the reach of detection by both Hayabusa2 and OSIRIS-REx at their respective targets. We anticipate this bias to be stronger for observations performed at smaller phase angles.

The serpentine UB-N sample was provided by the Service d'Analyse des Roches et des Minéraux (SARM) in Nancy, France. We thank J. Carter for providing us with the serpentine Rawhide and the saponite samples, which were purchased from Minerals Unlimited in Ridgecrest, California. We thank two anonymous reviewers for their useful remarks and suggestions. We are grateful to K. Kitazato, T. Nakamura, A. Aléon-Toppiani, Z. Djouadi, Y. Arribard, and R. Urso for helpful and useful discussions. We thank O. Mivumbi, D. Ledu, C.O. Bacri, and P. Benoit-Lamaitrie for help and technical support with SIDONIE and INGMAR. INGMAR is a joint IAS-CSNSM (Orsay, France) facility funded by the P2IO LabEx (ANR-10-LABX-0038) in the framework Investissements d'Avenir (ANR-11-IDEX-0003-01). The ex situ microspectroscopy measurements were supported by grants from Region Ile-de-France (DIM-ACAV) and SOLEIL. This work has been funded by the Centre National d'Etudes Spatiales (CNES-France) and by the ANR project CLASSY (Grant ANR-17-CE31-0004-02) of the French Agence Nationale de la Recherche.

Appendix

In addition to the in situ INGMAR measurements, we acquired additional ex situ measurements with two other instruments (spectra are shown in Figure A1): a PerkinElmer point spectrometer (left) and an Agilent microspectrometer (right). Both data sets were acquired with a Global source, with a spectral resolution of $4\ \text{cm}^{-1}$. Differences in the shape of the $2.7\ \mu\text{m}$ feature compared to the INGMAR measurements are due to the influence of the different optical geometries, which characterize each instrument, and the different contributions of adsorbed water.

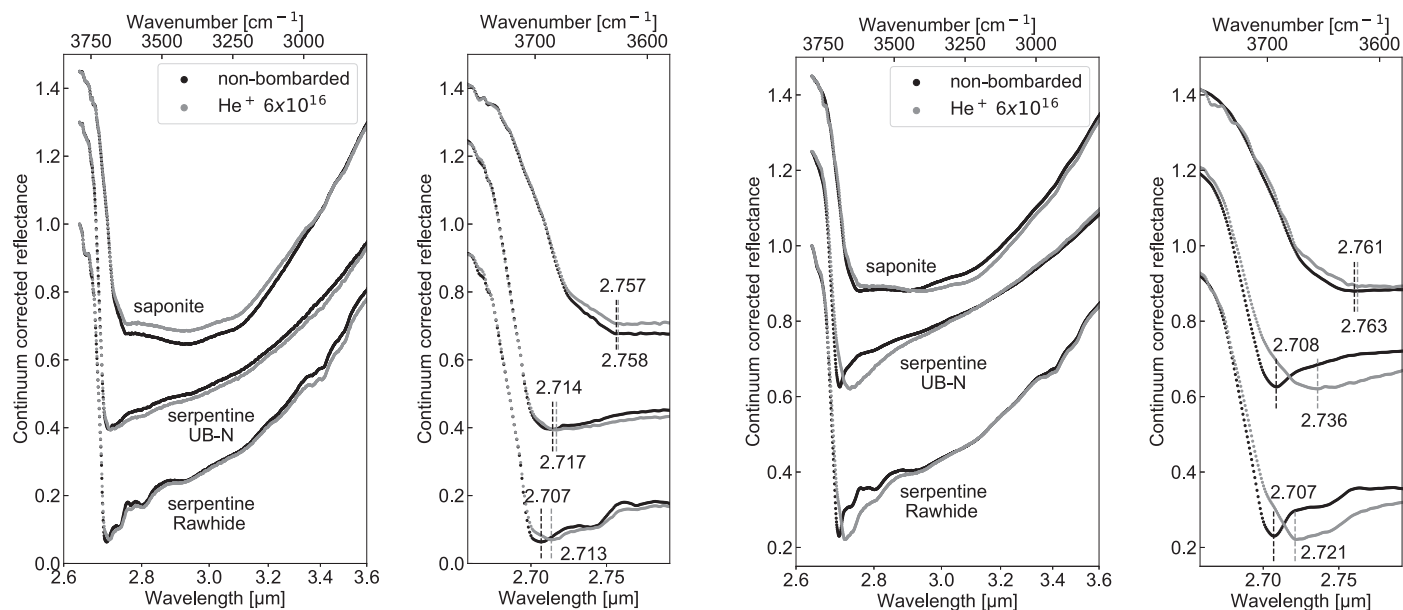


Figure A1. Ex situ evolution of the 2.7 μm feature before (virgin; black dots) and after maximum ion fluence (gray). Spectra were acquired at ambient pressure with two different setups: the PerkinElmer point spectrometer (left) and the Agilent IR microscope (right). For plotting, a linear scale is used with respect to wavenumbers. A linear continuum correction from 2.64 μm to 4 μm was applied. Right panels for each pair are zoomed in around the center of the bands plotted in the left panel.

ORCID iDs

Stefano Rubino <https://orcid.org/0000-0003-3198-1123>
 Catinel Lantz <https://orcid.org/0000-0003-0974-4770>
 Donia Baklouti <https://orcid.org/0000-0002-2754-7829>
 Hugues Leroux <https://orcid.org/0000-0002-8806-8434>
 Rosario Brunetto <https://orcid.org/0000-0003-3001-9362>

References

- Adams, J. B., & Filice, A. L. 1967, *JGR*, **72**, 5705
 Arakawa, M., Saiki, T., Wada, K., et al. 2020, *Sci*, **368**, 67
 Auzende, A.-L. 2003, PhD thesis, Laboratoire Magmas et Volcans, <https://hal.univ-grenoble-alpes.fr/LMV/tel-00825144>
 Besson, G., & Drits, V. A. 1997, *CCM*, **45**, 158
 Binzel, R. P., Rivkin, A. S., & Bus, S. J. 2001, *M&PS*, **36**, 36
 Bishop, J. L., Lane, M. D., Dyar, M. D., & Brown, A. J. 2008, *CIMin*, **43**, 35
 Bonal, L., Brunetto, R., Beck, P., et al. 2015, *M&PS*, **50**, 1562
 Brearley, A. J. 2006, in *Meteorites and the Early Solar System II*, ed. D. S. Lauretta & H. Y. McSween, Jr. (Tucson, AZ: Univ. Arizona Press), 585
 Brunetto, R., Lantz, C., Dionnet, Z., et al. 2018, *P&SS*, **158**, 38
 Brunetto, R., Lantz, C., Ledu, D., et al. 2014, *Icar*, **237**, 278
 Brunetto, R., Lantz, C., Nakamura, T., et al. 2020, *Icar*, **345**, 113722
 Brunetto, R., Loeffler, M. J., Nesvorný, D., Sasaki, S., & Strazzulla, G. 2015, in *Asteroids IV*, ed. P. Michel, F. E. DeMeo, & W. F. Bottke (Tucson, AZ: Univ. Arizona Press), 597
 Christensen, P. R., Hamilton, V. E., Mehall, G. L., et al. 2018, *SSRv*, **214**, 87
 Clark, B. E., Hapke, B., Pieters, C., & Britt, D. 2002, in *Asteroids III*, ed. W. F. Bottke, Jr. et al. (Tucson, AZ: Univ. Arizona Press), 585
 Clark, B. E., Lucey, P., Helfenstein, P., et al. 2001, *M&PS*, **36**, 1617
 de Sanctis, M. C., Ammannito, E., Raponi, A., et al. 2015, *Natur*, **528**, 241
 Delbo, M., Guy, L., Justin, W., et al. 2014, *Natur*, **508**, 233
 Farmer, V. C. 1974, *The Infrared Spectra of Minerals*, Vol. 4 (London: Mineralogical Society of Great Britain and Ireland)
 Gayk, T., & Kleinschrodt, R. 2000, *JMetG*, **18**, 293
 Hamilton, V. E., Simon, A. A., Christensen, P. R., et al. 2019, *NatAs*, **3**, 332
 Hamilton, V. E., Simon, A. A., Kaplan, H. H., et al. 2020, in *51st Lunar and Planetary Science Conf. (The Woodlands, TX)*, 1049
 Hapke, B., Cassidy, W., & Wells, E. 1975, *Moon*, **13**, 339
 Hiroi, T., Masanao, A., Kohei, K., et al. 2006, *Natur*, **443**, 56
 Iwata, T., Kohei, K., Masanao, A., et al. 2017, *SSRv*, **208**, 317
 Johnson, R. E. 1990, in *Energetic charged-Particle Interactions with Atmospheres and Surfaces, Physics and Chemistry in Space Planatology*, Vol. 19, ed. L. J. Lanzerotti, M. Hill, & D. Stoffer Munster (Berlin: Springer), 232
 King, A. J., Schofield, P. F., Howard, K. T., & Russell, S. S. 2015, *GeCoA*, **165**, 148
 Kitazato, K., Milliken, R. E., Iwata, T., et al. 2019, *Sci*, **364**, 272
 Kitazato, K., Milliken, R. E., Iwata, T., et al. 2020, *NatAs*, submitted
 Lantz, C., Brunetto, R., Barucci, M. A., et al. 2015, *A&A*, **577**, A41
 Lantz, C., Brunetto, R., Barucci, M. A., et al. 2017, *Icar*, **285**, 43
 Lantz, C., Clark, B. E., Barucci, M. A., & Lauretta, D. S. 2013, *A&AS*, **554**, A138
 Lauretta, D. S., Balram-Knutson, S. S., Beshore, E., et al. 2017, *SSRv*, **212**, 925
 Lebofsky, L. A. 1978, *MNRAS*, **182**, 17P
 Madejová, J., Gates, W. P., & Petit, S. 2017, *Developments in Clay Science*, Vol. 8 (Amsterdam: Elsevier), 107
 Marchi, S., Delbo, M., Morbidelli, A., Paolicchi, P., & Lazzarin, M. 2009, *MNRAS*, **400**, 147
 Matsumoto, T., Akira, T., Akira, M., et al. 2015, *Icar*, **257**, 230
 Mitra, S., Prabhudesai, S. A., Chakrabarty, D., et al. 2013, *PhRvE*, **87**, 062317
 Miyamoto, M., & Zolensky, M. E. 1994, *Metic*, **29**, 849
 Noguchi, T., Makoto, K., Takahito, H., et al. 2014, *M&PS*, **49**, 188
 Rivkin, A. S., Howell, E. S., Vilas, F., & Lebofsky, L. A. 2002, in *Asteroids III*, ed. W. F. Bottke, Jr. et al. (Tucson, AZ: Univ. Arizona Press), 235
 Roberts, W. L., Thomas, J. C., George, R. R., et al. 1990, *Encyclopedia of Minerals* (New York: Van Nostrand Reinhold)
 Rodriguez, M. A. V. 1994, *CCM*, **42**, 724
 Sabins, F. F. 1999, *Ore Geology Reviews*, **14**, 157
 Skinner, B. J. 1963, *Sci*, **139**, 821
 Takir, D., Joshua, P. E., Harry, Y. M., et al. 2013, *M&PS*, **48**, 1618
 Trombetta, M., Guido, B., Maurizio, L., et al. 2000, *Applied Catalysis A: General*, **193**, 9
 Urso, R. G., Donia, B., Zahia, D., Noemí, P.-A., & Rosario, B. 2020, *ApJL*, **894**, L3
 Vernazza, P., Binzel, R. P., Rossi, A., Fulchignoni, M., & Birlan, M. 2009, *Natur*, **458**, 993
 Vernazza, P., Fulvio, D., Brunetto, R., et al. 2013, *Icar*, **225**, 517
 Watanabe, S.-I., Yuichi, T., Makoto, Y., et al. 2017, *SSRv*, **208**, 3
 Ziegler, J. F., Ziegler, M. D., & Biersack, J. P. 2010, *NIMPB*, **268**, 1818
 Zolensky, M., & McSween, H. Y., Jr. 1988, in *Meteorites and the Early Solar System*, Vol. 14 (Tucson, AZ: Univ. Arizona Press), 114